Appl. Phys. A (2016)122:407
DOI 10.1007/s00339-016-9944-7

Applied Physics A
Materials Science & Processing

Experimental characterization and atomistic modeling of interfacial void formation and detachment in short pulse laser processing of metal surfaces covered by solid transparent overlayers

Eaman T. Karim[1] · Maxim V. Shugaev[1] · Chengping Wu[1] · Zhibin Lin[2] · Hisashi Matsumoto[2] · Maria Conneran[2] · Jan Kleinert[2] · Robert F. Hainsey[2,3] · Leonid V. Zhigilei[1]

Received: 17 October 2015 / Accepted: 28 February 2016

Abstract The short pulse laser interaction with metal surfaces covered by solid transparent overlayers is investigated in experiments and atomistic simulations, with a particular aim of revealing the mechanisms responsible for structural modification of the metal–overlayer interfacial regions. Experimental characterization of Al–silica targets modified by single-pulse laser irradiation with the pulse duration of 10 ps reveals the transitions from the generation of extended interfacial voids with internal nanoscale surface roughness to the partial detachment of the overlayer from the metal substrate, and to the cracking/chipping or complete removal of the overlayer as the laser fluence increases. The mechanisms responsible for the appearance, growth, and percolation of the interfacial voids leading to the detachment of the overlayer from the metal substrate are investigated in a large-scale atomistic simulation. The results of the simulation demonstrate that the processes of nucleation and growth of the interfacial voids are driven by the dynamic relaxation of laser-induced stresses proceeding simultaneously with rapid phase transformations and temperature variation in the interfacial region. The growth and coalescence of the interfacial voids results in the formation of liquid bridges connecting the overlayer and the metal substrate, whereas solidification of the transient liquid structures produced by the breakup of the liquid bridges may be responsible for the formation of the nanoscale roughness of the interfacial voids observed in experiments. Computational analysis of the effect of pre-existing interfacial voids reveals a complex dynamic picture of the initial expansion and subsequent compaction of the surface region of the metal substrate and suggests a possible scenario for the formation of voids below the metal–overlayer interface.

1 Introduction

The conditions of spatial confinement realized in short pulse laser interactions with an absorbing substrate covered by an optically transparent solid overlayer have a number of important implications on the materials response to the laser energy deposition, ranging from the enhancement of laser-induced pressure to the suppression of the ablation plume expansion and melt expulsion. The unique characteristics of the spatially confined laser interactions have attracted attention of the research community and have been demonstrated to be beneficial for a number of practical applications, such as laser shock peening [1–3], laser-induced forward transfer [4–6], thin film patterning/scribing [7, 8], and the generation of high-quality surface structures [9, 10].

The physical understanding of the effect of the spatial confinement on laser-induced processes is largely based on the results of theoretical analysis of the evolution of pressure generated under conditions of spatially confined laser ablation [2, 8] and continuum-level modeling of thermoelastic deformation of metal films irradiated through transparent substrates [3, 11, 12]. These studies have recently been complemented by atomistic molecular

✉ Leonid V. Zhigilei
lz2n@virginia.edu

[1] Department of Materials Science and Engineering, University of Virginia, 395 McCormick Road, Charlottesville, VA 22904-4745, USA

[2] Electro Scientific Industries, Inc., 13900 NW Science Park Drive, Portland, OR 97229, USA

[3] The International Society for Optics and Photonics, SPIE, Bellingham, WA 98227-0010, USA

Published online: 16 March 2016

dynamics (MD) simulations of short pulse laser interactions with bulk metal substrate covered by a solid transparent overlayer [13]. The atomistic simulations have provided important insights into the effect of the spatial confinement on the kinetics and mechanisms of laser-induced phase transformations. In particular, the spatial confinement is found to suppress the generation of unloading tensile wave, decrease the maximum depth of melting, prevent cavitation or spallation in the transiently melted region of the metal substrate, and create conditions for nucleation and growth of new crystallites at the metal–overlayer interface. At higher laser fluences, when the surface region of the metal substrate is brought into the supercritical state, the confinement by the overlayer prevents the expansion and phase decomposition of the supercritical fluid, which undergoes rapid cooling to the liquid state, contraction, and detachment from the overlayer. The relatively small lateral size of the computational systems used in the first simulations [13], however, prevented detailed analysis of some of the important processes inferred from the simulation results, such as the evolution of voids leading to the detachment at the metal–overlayer interface or the nucleation and growth of multiple crystallites leading to the formation of nanocrystalline structure in the interfacial region.

In the study reported in the present paper, we extend the initial computational analysis of Ref. [13] to a larger system and perform MD simulations targeted at revealing the microscopic mechanisms responsible for the formation of interfacial voids and/or partial detachment of the overlayer from the metal substrate. The laser-induced processes in the presence of preexisting interfacial voids generated by previous laser pulses or produced in the course of the deposition of the overlayer are also investigated in an MD simulation. The computational analysis of the generation of interfacial voids is supplemented by a systematic experimental characterization of laser-induced modification of Al substrates covered by silica overlayers. The results of the experimental investigation are discussed first, in Sect. 2, and are followed by presentation of computational predictions in Sect. 3 and a brief summary of the main conclusions of the combined experimental and computational study in Sect. 4.

2 Experimental characterization of laser modification of metal–overlayer targets

The experimental study is performed for an Al substrate covered by a silica overlayer. The sample used in the experiments has lateral dimensions of 5.1 × 5.1 cm^2 and a thickness of 1 mm. It is prepared by cold rolling of an Al (3003-H14) plate resulting in a surface roughness of approximately 1 μm, followed by chemical vapor deposition of a 10-μm-thick silica coating. Single-pulse irradiation of different areas on the sample is performed by IR 1064 nm laser system at five incident laser fluences of 0.97, 1.15, 1.28, 3.84, and 7.69 J/cm^2, with a laser pulse duration of 10 ps, and a Gaussian 1/e^2 laser spot diameter of 50 μm.

The nature and the extent of the laser-induced structural modification/damage of the metal substrate and the overlayer are characterized by optical and scanning electron microscopies. The images obtained by focusing the optical microscope on the outer surface of the silica overlayer and the metal–overlayer interface are shown in Fig. 1a, b, respectively. From the visual analysis of these images, one can identify the laser-affected zones as regions of the interface with altered optical properties. As expected, the size of the laser-affected zones increases with increasing laser fluence. No surface damage to the silica overlayer is observed at the three lower laser fluences (0.97, 1.15, and 1.28 J/cm^2), whereas a partial removal and a complete ablation of the overlayer can be seen at the two highest laser fluences of 3.84 and 7.69 J/cm^2, respectively.

The scanning electron microscopy (SEM) images reveal more detailed information on the nature of the laser-induced structural modification or damage to the targets. The SEM images of the vertical cross sections of the irradiated spots prepared by focused-ion-beam (FIB) milling are shown in Fig. 2a–e for incident fluences of 0.97 and 3.84 J/cm^2. At the lowest fluence of 0.97 J/cm^2, the laser-induced changes are limited to the generation of elongated micron-scale voids at the Al–silica interface. The voids observed in the central part of the spot (Fig. 2a) are larger than the ones at the spot edge (Fig. 2b) and result in a partial detachment of the overlayer from the metal substrate. Interestingly, some of the small voids appear inside the Al substrate, just beneath the Al–overlayer interface. The SEM images also reveal the presence of nanoscale roughness or nanoparticles on the surface of large voids, as can be seen in the enlarged view of the largest void shown in Fig. 2c. The mechanisms of the void formation and the origin of the nanoscale roughness are investigated in the simulations discussed in Sect. 3.

As the laser fluence increases, the size of the voids and the area affected by the detachment also increase, as can be seen from the SEM images shown in Fig. 2d, e for a laser fluence of 3.84 J/cm^2. Moreover, the irradiation at this fluence also damages the silica overlayer and creates an approximately 5.5-μm-deep crater at the outer surface of the overlayer. Since the laser fluence of 3.84 J/cm^2 is substantially lower than the damage threshold in bulk fused silica [14], the partial removal of the overlayer cannot be attributed to the direct optical damage in the

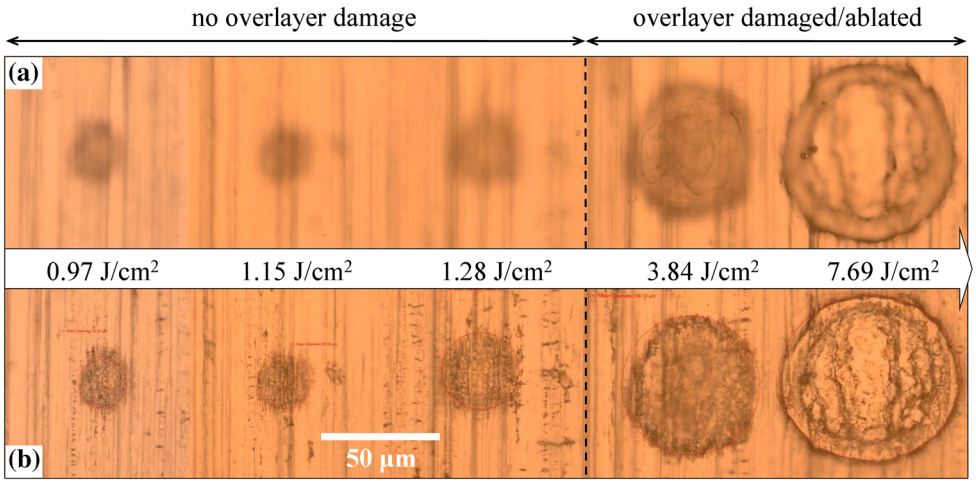

Fig. 1 Optical microscope images obtained by focusing microscope lenses on the surface of silica overlayer (**a**) and the Al–overlayer interface (**b**) of Al–silica samples irradiated by 10 ps laser pulses at five incident laser fluences indicated in the figure. The *black dashed line* separates the irradiation conditions that do not result in any visible damage to the overlayer from the ones when cracking/chipping or complete removal of the overlayer is observed. The nature of the target modification is further illustrated by SEM images shown in Fig. 2

fused silica. A plausible explanation of the damage to the overlayer may be proposed based on the results of the simulations discussed below, in Sect. 3, which suggest that a high, on the order of tens of GPa, compressive pressure is generated near the metal surface by the spatially confined laser excitation. A compressive wave driven by the relaxation of laser-induced pressure propagates from the interfacial region towards the surface of the overlayer, transforms into tensile wave upon reflection from the free surface of the overlayer and may cause spallation when the magnitude of the tensile wave exceeds the dynamic strength of the silica glass [15].

At the highest laser fluence of 7.69 J/cm^2, the pressure created by the laser excitation of the metal substrate is sufficiently high to completely remove the 10-µm-thick silica overlayer, as can be seen from Fig. 2f, g. The removal of the overlayer makes it possible for the hot metal region to expand and undergo rapid decomposition into vapor and liquid droplets, similar to ablation in a background gas environment or in vacuum. The explosive decomposition and ejection of a top part of the metal substrate create conditions for rapid cooling and solidification of the remaining target. The rapid solidification, in turn, freezes transient liquid structures generated in the ablation process [16, 17] and results in the formation of complex surface morphology featuring nanospikes and ripples that are similar to the ones commonly produced by laser processing in air or vacuum, e.g., [18–20].

3 Atomistic simulation of interfacial void formation

The dynamic processes responsible for the generation of the interfacial voids and partial detachment of the overlayer from the metal substrate are investigated in a large-scale MD simulation performed for a Ag substrate covered by a thick silica glass overlayer. The choice of Ag rather than Al used in the experiments described in Sect. 2 is determined by the availability of the results of smaller scale atomistic simulations performed for the Ag–silica system, which have already identified the irradiation regime where the overlayer detachment can be expected to occur [13]. We note, however, that the phenomena of the generation of interfacial voids and detachment of a transparent overlayer from an absorbing substrate appear to be general and have been observed for various systems, such as a Si substrate covered by a thermally grown native oxide layer [21], or Ni and Si substrates covered by polymer confinement layers [9]. Therefore, we expect the computational insights into the mechanisms of the interfacial void formation to be applicable to various material systems where a confinement layer is used to control the laser processing conditions.

3.1 Computational model

The computational setup used in the atomistic simulations of laser interactions with a bulk Ag target covered by a solid transparent overlayer is schematically illustrated in

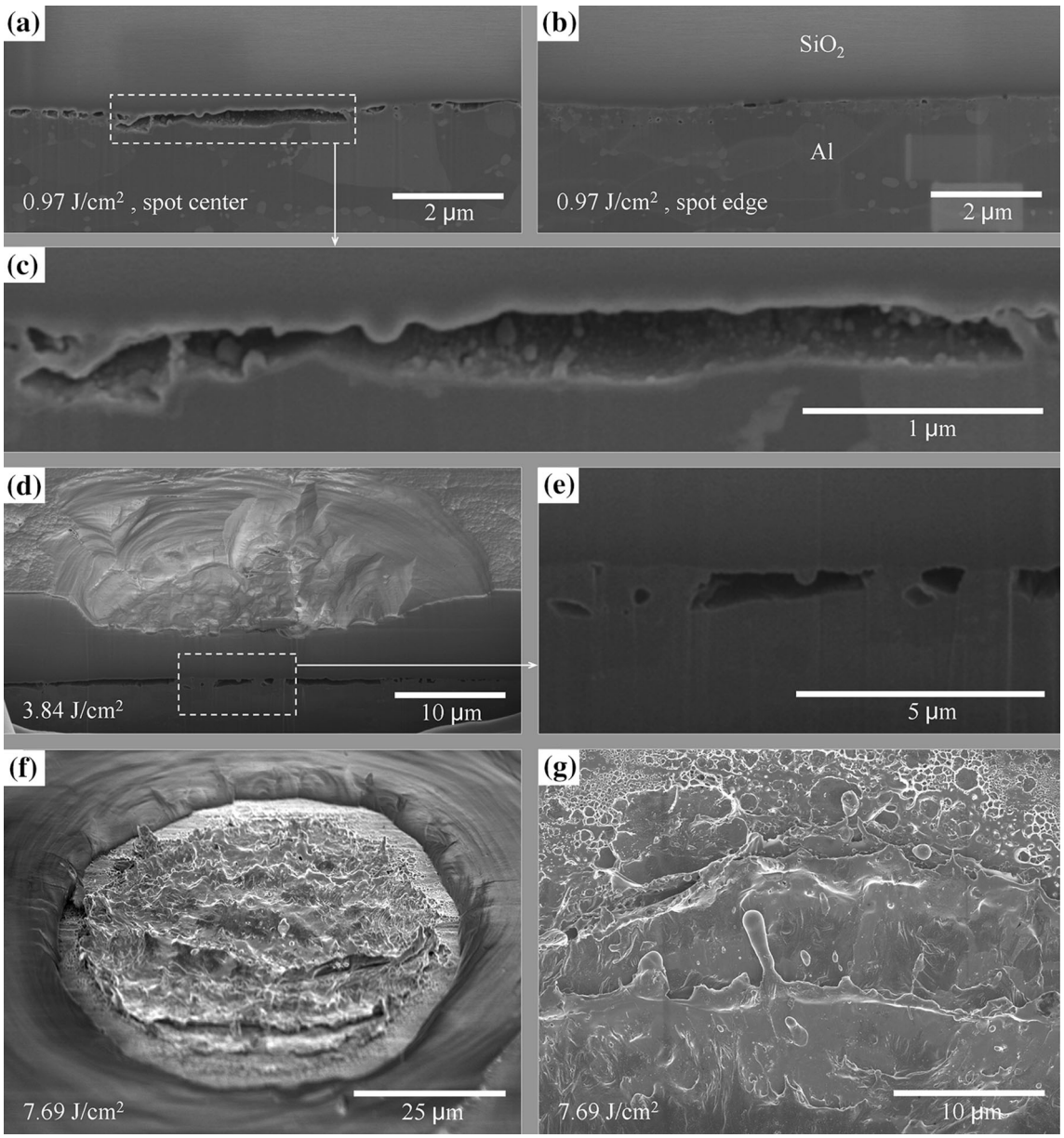

Fig. 2 SEM images of Al–silica samples irradiated by 10 ps laser pulse at three incident laser fluences of 0.97 J/cm^2 (**a**–**c**), 3.84 J/cm^2 (**d**, **e**), and 7.69 J/cm^2 (**f**, **g**). The images in **a–e** show *vertical cross sections* of the irradiated spots prepared by FIB milling that reveal the interfacial voids and partial detachment at the metal–overlayer interface. The images in **f**, **g** show the metal surface exposed by complete removal of the overlayer at a fluence of 7.69 J/cm^2

Fig. 3. The top part of the Ag target, down to the depth of $L^z_{\mathrm{TTM-MD}}$ under the metal–overlayer interface, is represented by a hybrid computational model [22] combining the classical MD method with a continuum-level description of the laser excitation and subsequent relaxation of the conduction band electrons based on so-called two-temperature model (TTM) [23]. The heat conduction in the deeper part of the substrate, down to the depth of $L^z_{\mathrm{TTM-MD}} + L^z_{\mathrm{TTM}}$, is simulated with the conventional TTM equations. A L^z_{MD}-thick part of the transparent overlayer adjacent to the metal substrate is simulated with a MD model adopting a pairwise potential fitted to provide an adequate description of the experimental values of elastic constants, melting temperature, and density of fused silica, as well as the work of adhesion at the Ag–silica interface [13]. The dynamic pressure-transmitting boundary conditions [13, 24, 25] are applied at the bottom of the TTM–MD region of the metal substrate and at the top of the MD part of the overlayer to simulate non-reflective propagation of the laser-induced pressure waves from the interfacial region to the bulk of the metal substrate and towards the surface of the overlayer, respectively. The reflection of the

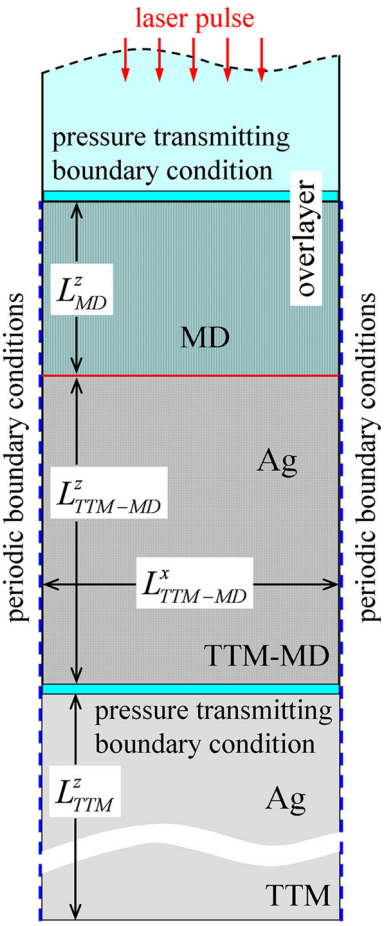

Fig. 3 Schematic sketch of the computational setup used in the simulations of laser interaction with a Ag target covered by a solid transparent overlayer. The top layer of the Ag target with thickness of $L^z_{\mathrm{TTM-MD}}$ is represented by the atomistic TTM–MD model, whereas the heat conduction in the deeper part of the substrate is simulated with TTM equations solved in an additional part of the target with thickness of L^z_{TTM}. A L^z_{MD}-thick part of the transparent overlayer adjacent to the metal substrate is represented with a MD model, while the rest of the overlayer is not explicitly treated in the simulations. The dynamic pressure-transmitting boundary conditions are applied at the bottom of the TTM–MD region and at the top of the MD part of the overlayer to mimic non-reflective propagation of laser-induced pressure waves through the boundaries

pressure wave from the top surface of the overlayer is not considered in the simulations since the time required for the propagation of the wave through a 10 μm thick silica overlayer and back to the interfacial region is longer than the time-scale of the processes considered in the simulations. A complete description of the computational model is provided in Ref. [13], and below we only provide the parameters of the computational setup used in the simulations reported in this paper.

Taking advantage of the computationally efficient parallel implementation of the computational model, one of the simulations reported below, in Sect. 3.2, is performed for a large computational system composed of more than 330 million atoms. The lateral (parallel to the Ag–silica interface) dimensions of the system are $L^x_{\mathrm{TTM-MD}} = L^y_{\mathrm{TTM-MD}} = 100$ nm and periodic boundary conditions are applied in these directions. In the direction normal to the interface, the TTM–MD and MD representations of the Ag substrate and the silica overlayer extend to $L^z_{\mathrm{TTM-MD}} = 500$ nm for Ag (~303 million atoms) and $L^z_{\mathrm{MD}} = 200$ nm for silica (~27 million atoms) from the interface. In another simulation, targeted at evaluation of the effect of preexisting interfacial voids on the laser induced processes and discussed in Sect. 3.3, a much smaller lateral size of the system, $L^x_{\mathrm{TTM-MD}} = L^y_{\mathrm{TTM-MD}} = 4.1$ nm, a thickness of the TTM–MD part of the Ag substrate of $L^z_{\mathrm{TTM-MD}} = 411$ nm (400,000 atoms), and a thickness of the MD part of the silica overlayer of $L^z_{\mathrm{MD}} = 137$ nm (28,800 atoms) are used.

In both simulations, the continuum part of the TTM–MD model, in which the electron heat conduction is described by the conventional TTM, is extended to the depth of $L^z_{\mathrm{TTM-MD}} + L^z_{\mathrm{TTM}} = 2.5$ μm from the metal–overlayer interface to ensure that no substantial temperature changes are observed at the bottom of the continuum region by the end of the simulation. The choice of the parameters used in the TTM equation for the electron temperature of Ag is explained in Ref. [26] and the interatomic interactions in the Ag part of the model are described by the embedded atom method (EAM) potential in the form proposed in Ref. [27], with a cutoff function [28] that smoothly brings the interaction energies and forces to zero at a cutoff distance of 5.5 Å added to the potential. Before applying the laser irradiation, the computational systems are equilibrated at 300 K for 200 ps.

The irradiation of the target with a 10 ps laser pulse is represented through a source term added to the TTM equation for the electron temperature [22]. The source term simulates excitation of the conduction band electrons by a laser pulse with a Gaussian temporal profile and reproduces the exponential attenuation of laser intensity with depth under the metal surface. To account for the energy transport occurring before the thermalization of the excited electrons, the optical absorption depth, 12 nm at laser wavelength of 1 μm [29], is combined with the effective depth of the "ballistic" energy transport, 56 nm, roughly estimated in Ref. [13] as a product of the Fermi velocity and the Drude relaxation time [30]. To ensure complete deposition of the energy of the 10 ps laser pulses, the peak intensity of the Gaussian laser pulse is shifted to 25 ps from the beginning of the simulations.

3.2 Generation of the interfacial voids and overlayer detachment

The physical processes responsible for the appearance, growth, and percolation of the interfacial voids leading to

the detachment of the overlayer from the metal substrate are discussed in this section based on the results of a large-scale simulation performed for irradiation conditions identified in smaller scale simulations [13] as conditions leading to the overlayer detachment. The metal–overlayer target is irradiated by a 10 ps laser pulse at an absorbed laser fluence of 0.4 J/cm^2, which is about twice higher than the threshold fluence for the onset of phase explosion in the case of laser ablation of a bare Ag target in vacuum. The uncertainty with respect to the reflectance of the metal–overlayer interfaces in experiments discussed in Sect. 2 does not allow us to reliably convert the values of the incident laser fluence to the absorbed fluence. At the semi-quantitative level, however, the conditions of the simulation performed at the absorbed fluence that is about 40–50 % above the threshold for the generation of the interfacial voids [13] can be expected to be comparable to the ones in the lower fluence experiments (incident fluences of 0.97–1.28 J/cm^2), where partial detachment at the interface (Fig. 2a–c) but no damage to the overlayer (Fig. 1) are observed.

The processes responsible for the structural modification of the metal–overlayer target are largely defined by the rapid evolution of temperature and pressure in the vicinity of the region of the laser energy deposition, shown in the form of contour plots in Fig. 4. Following the laser excitation of the conduction band electrons within the optical absorption depth of the Ag substrate, the energy of the excited electrons is rapidly redistributed through the ballistic and diffusive electron energy transport and transferred to the lattice vibrations due to the electron–phonon coupling. This energy transfer leads to a rapid temperature increase within ~200-nm-deep region of the metal substrate, Fig. 4a. The temperature quickly exceeds the limit of crystal stability against the onset of massive homogeneous meting [31, 32], triggering a rapid (within several picoseconds) collapse of the highly superheated crystal lattice. Additional slower melting down to the depth of ~340 nm below the Ag–overlayer interface then proceeds through the propagation of the melting front from the homogeneously melted part of the substrate and is assisted by the tensile stresses generated near the melting front [33], as shown in Fig. 4b and discussed below. Following the rapid melting, the temperature of liquid Ag adjacent to the interface continues to increase due to the energy transfer from the hot electrons and reaches the maximum of ~8200 K by 40 ps (15 ps after the time of the peak intensity of the Gaussian laser pulse), thus bringing the top part of the Ag substrate to the supercritical state.

The rapid temperature increase during the first 40 ps of the simulation takes place under conditions of stress confinement [34–38] and results in a buildup of strong compressive stresses, as can be seen from Fig. 4b. The

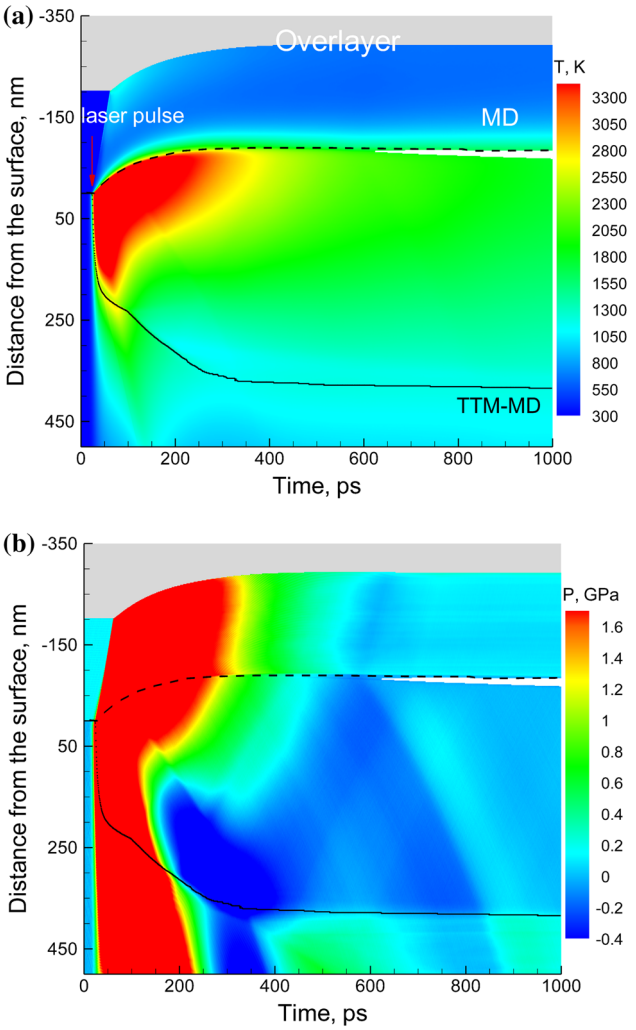

Fig. 4 Contour plots showing the spatial and temporal evolution of **a** temperature and **b** pressure predicted in a simulation of a Ag-overlayer target irradiated by a 10 ps laser pulse at an absorbed fluence of 0.4 J/cm^2. To ensure complete deposition of the laser energy, the peak intensity of the Gaussian laser pulse is shifted to 25 ps from the beginning of the simulation, as shown by the *red arrow* in (**a**). The *black solid curve line* separates the melted region from the crystalline part of the Ag target. The *black dashed line* tracks the location of the Ag–overlayer interface. The area where the density of the material drops below 10 % of the initial density of the solid Ag target is blanked in the plots

compressive pressure reaches the maximum level of ~30 GPa at a depth of ~60 nm below the interface by the time of 35 ps and then relaxes by expanding the hot region of the metal substrate and driving two compressive pressure waves, one propagating deeper into the metal substrate and another into the silica overlayer. In contrast to the laser ablation of a bare metal surface, where the expansion of the surface region proceeds in the form of an explosive decomposition of the superheated liquid into a mixture of vapor and liquid droplets [16, 34, 37–39], the phase decomposition is suppressed by the presence of the

overlayer, which maintains high pressure in the interfacial region. Thus, the supercritical fluid near the interface does not decompose but is gradually cooled to the liquid state by the electronic heat transfer to the bulk of the metal substrate.

Since the acoustic impedance of the overlayer material is more than twice smaller than the one of Ag, the expansion of the metal substrate against the softer overlayer also produces a weak unloading wave propagating from the interface to the bulk of the Ag substrate. Partial reflection of the unloading wave from the melting front generates a transient spike of the tensile stresses up to about -1.1 GPa near the solid–liquid interface, at a depth of ~ 330 nm. The relatively low temperature of liquid near the melting front (close to the equilibrium melting temperature of the EAM Ag at zero pressure, $T_m = 1139$ K [26]) and a short time of the spike of the tensile stresses preclude cavitation from taking place in the region of the maximum tensile stresses. When the reflected part of the tensile wave reaches the metal–overlayer interface at ~ 600 ps, however, the much lower tensile stresses of about -0.12 GPa do induce nucleation of voids in the interfacial region weakened by melting of ~ 10 nm part of the overlayer and relatively high temperature of the interfacial region, $\sim 1.7T_m$ at the time of the arrival of the tensile wave. The growth of the voids results in the appearance of a region of reduced density at the metal–overlayer interface that shows up as a white gap in the contour plots in Fig. 4. The growth of the voids is facilitated by continuous cooling and contraction of the top region of the metal substrate that contribute to the expansion of the cavitation zone, elongation of the liquid bridges connecting the metal substrate to the overlayer and eventual detachment of the overlayer.

A visual picture of the nucleation and growth of the voids at the Ag–overlayer interface is provided by a series of snapshots of atomic configurations shown in Fig. 5. The snapshots are shown for a 74 nm thick slice of the computational cell adjacent to the interface. The first snapshot is shown for a time of 600 ps, when a 10 nm deep part of the silica overlayer is melted and the first small voids appear at the Ag–overlayer interface in response to the

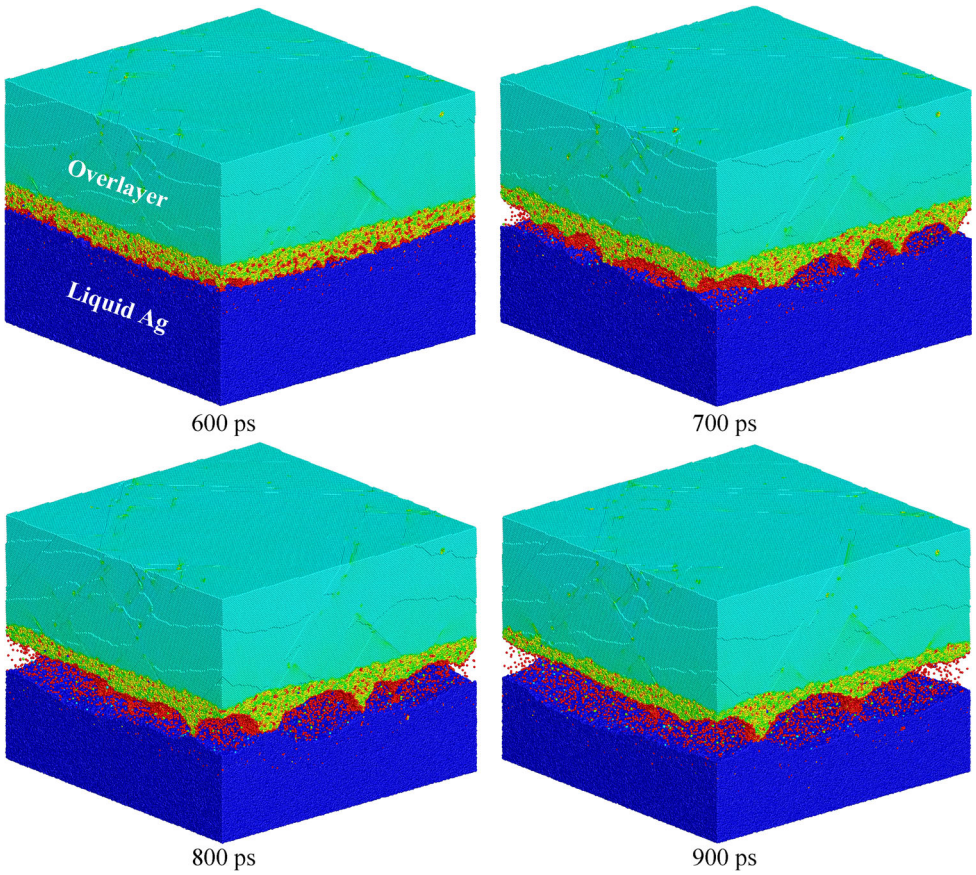

Fig. 5 Snapshots of atomic configurations obtained in a simulation of a Ag-overlayer target irradiated by a 10 ps laser pulse at an absorbed fluence of 0.4 J/cm^2. Only a 74-nm-thick slices of the computational system adjacent to the Ag–overlayer interface are shown in the snapshots. The atoms are *colored* according to their potential energies, so that the *dark blue color* represents liquid Ag, *turquoise* and *yellow/green colors* represent the solid and melted parts of the overlayer, respectively, and the vapor phase atoms are *red*

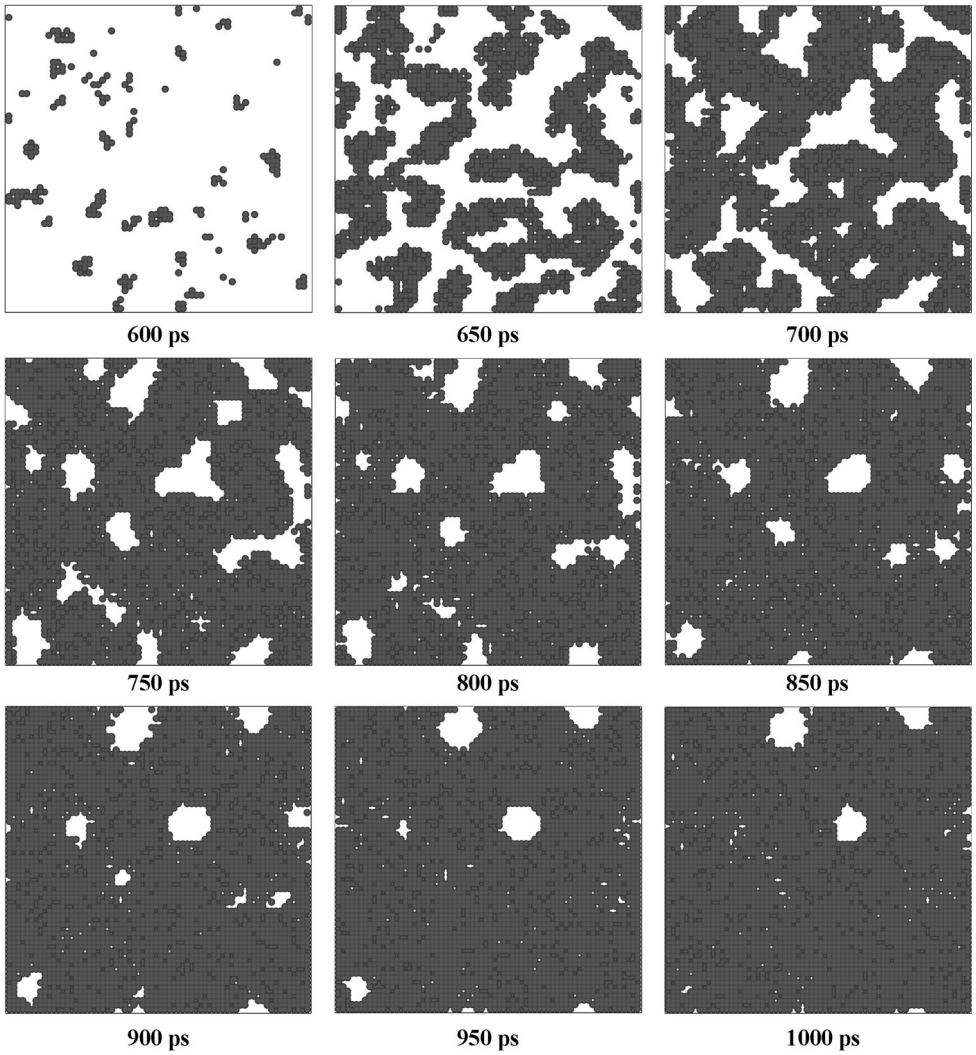

Fig. 6 Top-view projections of the voids evolving in the Ag-overlayer interfacial region in the simulation illustrated by Figs. 4 and 5. The *dark regions* show the areas where the material density drops below 10 % of the initial density of solid Ag, whereas the *white regions* represent the connections between the metal substrate and the overlayer. The size of the region shown in the snapshots corresponds to the lateral size of the computational system, 100 nm × 100 nm

raise of the tensile stresses (Fig. 4b). Gradually, growth and coalescence of the voids lead to the formation of liquid bridges connecting the overlayer and metal substrate, with some of the bridges breaking as the gap between the overlayer and the metal substrate grows. By the end of the simulation at 1 ns, three liquid bridges still connect the overlayer with the Ag substrate. Note that although vapor-phase atoms can be clearly seen to fill up the cavitation region, the vapor pressure of 1.7 MPa, estimated from the temperature and density of the vapor in the ideal gas approximation, is negligible as compared to the variation of pressure shown in Fig. 4b. The generation and growth of the interfacial voids, therefore, can be squarely attributed to the dynamic relaxation of the laser-induced stresses proceeding simultaneously with rapid expansion and contraction of the superheated surface region of the metal substrate, with the release of the vapor playing an insignificant role.

The evolution of the voids in the interfacial region is further illustrated in Fig. 6, where top-view projections of all the voids are shown. The voids are identified by dividing the computational cell into small cubic boxes with volumes of 3.4 nm^3 and defining voids as regions composed of boxes with density lower than 10 % of the initial density of Ag. The voids are then plotted in Fig. 6 as dark regions, whereas the white regions represent the liquid bridges connecting the Ag substrate with the overlayer. As discussed above, the nucleation of small voids at $\sim$600 ps coincides with the arrival of the tensile wave to the Ag–overlayer interface and the contraction of the top part of the

metal substrate due to the cooling process. Following the nucleation, the voids grow and coalesce, thus reducing the number and the total cross-sectional area of the connecting liquid bridges.

The formation of the interfacial voids and partial detachment of the overlayer from the metal substrate are consistent with experimental observations presented in Sect. 2. The formation of the liquid bridges connecting the metal substrate with the overlayer may be responsible for generation of the nanoscale roughness on the surface of large voids observed in experiments, Fig. 2c. While the relatively weak adhesion between the silica overlayer and Ag leads to the early breakup of the liquid bridges in the simulation (the three remaining bridges observed in the simulation at 1 ns are likely to break up upon further expansion of the gap between the metal substrate and overlayer), a stronger metal–silica interaction and the restraining effect of the colder periphery of the laser spot, where the conditions for the detachment are not achieved, on the outward motion of the central part of the overlayer may stabilize the bridges and facilitate nucleation of some of the voids below the metal–overlayer interface. The solidification process may then capture the voids/bridges, solidify the transient surface roughness generated by the evolving liquid bridges, and produce the interfacial structures shown in the experimental images in Fig. 2. An additional scenario for the generation of voids inside the metal substrate, below the metal–overlayer interface, can be suggested based on the results of a simulation of laser interaction with a system containing a preexisting interfacial void that is described below.

3.3 The effect of preexisting interfacial voids

In contrast to the perfect metal–overlayer interface considered in the previous section, real experimental samples may contain small interfacial gaps or voids formed in the process of sample preparation. Moreover, the voids generated by prior laser pulses may affect the response of the target to irradiation by subsequent laser pulses in the multipulse irradiation regime. To investigate the effect of preexisting interfacial voids on the laser-induced processes, a simulation of a system with a 50-nm gap between the transparent overlayer and Ag substrate has been performed for a smaller computational system (lateral size of 4.1 nm × 4.1 nm) and the same irradiation condition as in the simulation discussed above, in Sect. 3.2.

The evolution of temperature, pressure and density in the irradiated system is presented in Fig. 7. The presence of the void makes it possible for the hot metal region to expand and generate an unloading wave propagating from the interfacial region and initiating the material decomposition down to the depth ~180 nm. As a result, the initial

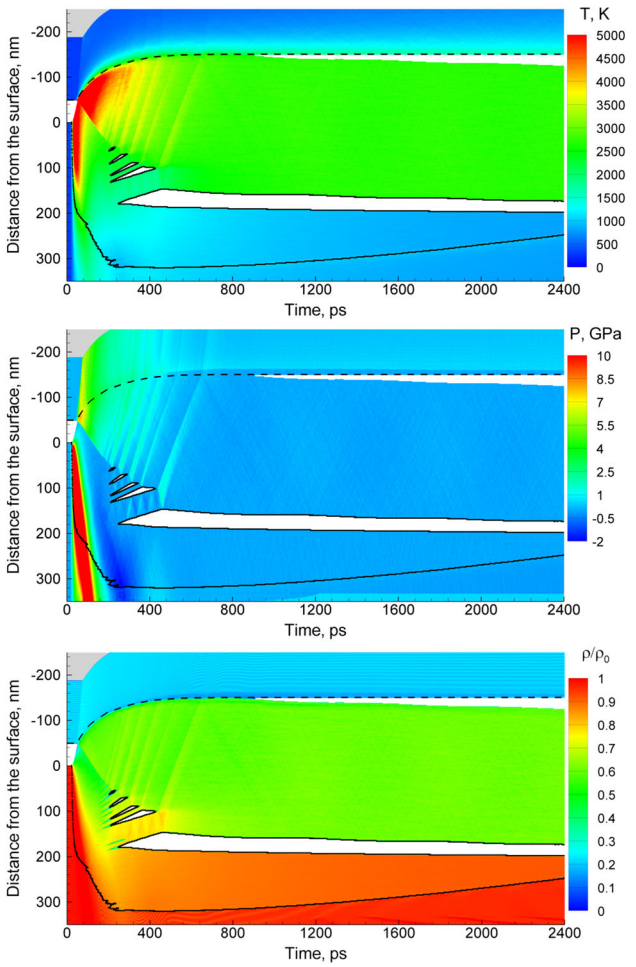

Fig. 7 Temperature, pressure and density contour plots obtained in a simulation of bulk Ag substrate covered by a transparent overlayer with an initial 50 nm thick gap between the overlayer and the Ag substrate. The Ag-overlayer target is irradiated by a 10 ps laser pulse at an absorbed laser fluence of 0.4 J/cm^2. Areas where the density of the material drops below 10 % of the initial density of the solid Ag target are blanked in the plots. The *black curves* outline voids inside the material and separate the melted region from the crystalline part of the Ag target. The *black dashed line* shows the position of the Ag–overlayer interface

stage of the material response to the laser excitation is similar to the one of a target with a free surface, when the top surface region undergoes an explosive decomposition into a mixture of vapor and small droplets while the generation of voids in a deeper and colder melted region is driven by the tensile stresses associated with the unloading wave [16, 34, 38]. In the present simulation, however, the collision of the ejected material with the overlayer interrupts the expansion of the ablation plume, converts the kinetic energy of directed motion of the plume into thermal energy, and creates highly energetic supercritical fluid with the maximum temperature and pressure values reaching 10,000 K and 8 GPa by the time of 70 ps.

The pressure exerted by the hot supercritical metal pushes the overlayer up by $\sim$100 nm and launches a compaction wave that stops the material decomposition initiated by the unloading wave and leads to the collapse of all but the deepest subsurface voids generated in the course of the initial material expansion. Each of the collapsing voids generates a pressure pulse consisting of compressive and unloading/tensile components that can be seen in the pressure contour plot in Fig. 7. The initial electronic heat transfer to deeper regions of the metal substrate combined with the fluid expansion and the energy loss on the mechanical work spent on displacing the overlayer (the latter can be estimated to be on the order of 400 J/m^2, which roughly corresponds to the thermal energy change upon cooling of a 50 nm Ag layer by $\sim$2500 K) leads to a rapid cooling of the interfacial part of the metal substrate from the supercritical state with temperature of $\sim 10^4$ K down to the regular liquid with a temperature of 2700 K by the time of 900 ps.

At 900 ps, the combined effect of the contraction of the rapidly cooled liquid Ag and an arrival of a weak tensile stress wave generated at the onset of the collapse of the last void (the maximum tensile stresses at the interface reach the level of about -50 MPa at 850 ps) results in the detachment of the metal substrate from the overlayer at the interface. Given the slower ($\sim$11 m/s) downward motion of the detached liquid layer as compared to the faster ($\sim$56 m/s) advancement of the solidification front, one can expect the solidification front to reach the location of the void $\sim$1.5 ns earlier. While the small lateral size of the computational system used in this simulation does not allow us to simulate the void capture and stabilization by the solidification front, such process has been observed in larger-scale simulations of laser interaction with an Ag target in vacuum [40]. Thus, the results of the simulation discussed above indicate that the presence of preexisting interfacial voids may facilitate generation of voids at some depth below the interface, as observed in experimental images, e.g., Fig. 2e.

4 Summary

The characteristic features of short pulse laser processing of metal surfaces under conditions of spatial confinement by a solid transparent overlayer are investigated in experiments and atomistic simulations, with a particular focus on establishing the mechanisms responsible for the formation of interfacial voids and/or partial detachment of the overlayer from the metal substrate. The dependence of the nature of the laser-induced structural modification and/or damage of the metal–overlayer target on the incident laser fluence is characterized experimentally for Al substrates covered by silica overlayers. At laser fluences that are close to the threshold for the interfacial void formation, the SEM images reveal the presence of nanoscale roughness on the surface of elongated interfacial voids, formation of small voids inside the metal substrate, and partial detachment of the overlayer from the substrate in the central region of the laser spot. The increase in the laser fluence leads to the increase in the size of the voids, expansion of the area affected by the detachment and, eventually, to the cracking/chipping or complete removal of the overlayer.

The physical processes responsible for the appearance, growth, and percolation of the interfacial voids leading to the detachment of the overlayer from the metal substrate are investigated in a large-scale atomistic simulation performed for a Ag substrate covered by a thick silica glass overlayer. The results of the simulations demonstrate that the generation and growth of the interfacial voids is driven by the dynamic relaxation of laser-induced stresses proceeding simultaneously with rapid phase transformations and temperature variation in the interfacial region. The initial expansion of the top region of the metal substrate brought to the supercritical state by the laser energy deposition turns to the contraction caused by the rapid cooling of the interfacial region down to the liquid state. The contraction of the interfacial region combined with additional tensile stresses produced by the arrival of an unloading wave generated at the metal–overlayer interface and partially reflected from the melting front is leading to the void nucleation and growth in the interfacial region. The growth and coalescence of the interfacial voids results in the formation of liquid bridges connecting the overlayer and metal substrate, whereas solidification of the transient liquid structures produced by the breaking bridges may be responsible for the formation of the nanoscale roughness of the internal surfaces of interfacial voids observed in experiments. The results of an additional simulation performed for a system containing a preexisting interfacial void reveal a complex dynamics of the initial expansion and subsequent compaction of the surface region of the metal substrate and suggest a possible scenario for the formation of voids inside the metal substrate, below the metal–overlayer interface.

Acknowledgments Financial support for this work was provided by the National Science Foundation (NSF) through Grant CMMI-1301298, the Air Force Office of Scientific Research through Grant FA9550-10-1-0541, and Electro Scientific Industries, Inc. Computational support was provided by the Oak Ridge Leadership Computing Facility (Project MAT048) and NSF through the Extreme Science and Engineering Discovery Environment (Project TG-DMR110090). The authors at ESI thank Motoaki Honda of University of Oregon for kind assistance with SEM measurements.

References

1. B.P. Fairand, B.A. Wilcox, W.J. Gallagher, D.N. Williams, Laser shock-induced microstructural and mechanical property changes in 7075 aluminum. J. Appl. Phys. **43**, 3893 (1972)
2. R. Fabbro, J. Fournier, P. Ballard, D. Devaux, J. Virmont, Physical study of laser-produced plasma in confined geometry. J. Appl. Phys. **68**, 775 (1990)
3. X. Wu, Z. Duan, H. Song, Y. Wei, X. Wang, C. Huang, Shock pressure induced by glass-confined laser shock peening: Experiments, modeling and simulation. J. Appl. Phys. **110**, 053112 (2011)
4. J. Bohandy, B.F. Kim, F.J. Adrian, Metal deposition from a supported metal film using an excimer laser. J. Appl. Phys. **60**, 1538 (1986)
5. I. Zergioti, S. Mailis, N.A. Vainos, C. Fotakis, S. Chen, C.P. Grigoropoulos, Microdeposition of metals by femtosecond excimer laser. Appl. Surf. Sci. **127–129**, 601 (1998)
6. M. Domke, S. Rapp, M. Schmidt, H.P. Huber, Ultra-fast movies of thin-film laser ablation. Appl. Phys. A **109**, 409 (2012)
7. G. Heise, M. Englmaier, C. Hellwig, T. Kuznicki, S. Sarrach, H.P. Huber, Laser ablation of thin molybdenum films on transparent substrates at low fluences. Appl. Phys. A **102**, 173 (2011)
8. G. Heise, M. Domke, J. Konrad, S. Sarrach, J. Sotrop, H.P. Huber, Laser lift-off initiated by direct induced ablation of different metal thin films with ultra-short laser pulses. J. Phys. D.: Appl. Phys. **45**, 315303 (2012)
9. J.-H. Klein-Wiele, P. Simon, Sub-100 nm pattern generation by laser direct writing using a confinement layer. Opt. Express **21**, 9017 (2013)
10. J. Ihlemann, R. Weichenhain-Schriever, Pulsed laser-induced formation of silica nanogrids. Nanoscale Res. Lett. **9**, 102 (2014)
11. J. Sotrop, A. Kersch, M. Domke, G. Heise, H.P. Huber, Numerical simulation of ultrafast expansion as the driving mechanism for confined laser ablation with ultra-short laser pulses. Appl. Phys. A **113**, 397 (2013)
12. M.V. Shugaev, N.M. Bulgakova, Thermodynamic and stress analysis of laser-induced forward transfer of metals. Appl. Phys. A **101**, 103 (2010)
13. E.T. Karim, M. Shugaev, C. Wu, Z. Lin, R.F. Hainsey, L.V. Zhigilei, Atomistic simulation study of short pulse laser interactions with a metal target under conditions of spatial confinement by a transparent overlayer. J. Appl. Phys. **115**, 183501 (2014)
14. A.V. Smith, B.T. Do, Bulk and surface laser damage of silica by picosecond and nanosecond pulses at 1064 nm. Appl. Opt. **47**, 4812 (2008)
15. J. Cagnoux, F. Longy, Spallation and shock-wave behaviour of some ceramics. J. Phys. Colloq. **49**(C3), C3–3 (1988)
16. C. Wu, L.V. Zhigilei, Microscopic mechanisms of laser spallation and ablation of metal targets from large-scale molecular dynamics simulations. Appl. Phys. A **114**, 11 (2014)
17. C. Wu, L.V. Zhigilei, Nanocrystalline and polyicosahedral structure of a nanospike generated on metal surface irradiated by a single femtosecond laser pulse. J. Phys. Chem. C **120**, 4438 (2016)
18. A.Y. Vorobyev, C. Guo, Enhanced absorptance of gold following multipulse femtosecond laser ablation. Phys. Rev. B **72**, 195422 (2005)
19. J.-M. Savolainen, M.S. Christensen, P. Balling, Material swelling as the first step in the ablation of metals by ultrashort laser pulses. Phys. Rev. B **84**, 193410 (2011)
20. J.V. Oboňa, V. Ocelík, J.C. Rao, J.Z.P. Skolski, G.R.B.E. Römer, A.J. Huis in 't Veld, J.T.M. De Hosson, Modification of Cu surface with picosecond laser pulses. Appl. Surf. Sci. **303**, 118 (2014)
21. S. Hermann, N.-P. Harder, R. Brendel, D. Herzog, H. Haferkamp, Picosecond laser ablation of SiO_2 layers on silicon substrates. Appl. Phys. A **99**, 151 (2010)
22. D.S. Ivanov, L.V. Zhigilei, Combined atomistic-continuum modeling of short-pulse laser melting and disintegration of metal films. Phys. Rev. B **68**, 064114 (2003)
23. S.I. Anisimov, B.L. Kapeliovich, T.L. Perel'man, Electron emission from metal surfaces exposed to ultrashort laser pulses. Sov. Phys. JETP **39**, 375 (1974)
24. L.V. Zhigilei, B.J. Garrison, Pressure waves in microscopic simulations of laser ablation. Mater. Res. Soc. Symp. Proc. **538**, 491 (1999)
25. C. Schäfer, H.M. Urbassek, L.V. Zhigilei, B.J. Garrison, Pressure-transmitting boundary conditions for molecular-dynamics simulations. Comput. Mater. Sci. **24**, 421 (2002)
26. C. Wu, D.A. Thomas, Z. Lin, L.V. Zhigilei, Runaway lattice-mismatched interface in an atomistic simulation of femtosecond laser irradiation of Ag film–Cu substrate system. Appl. Phys. A **104**, 781 (2011)
27. S.M. Foils, M.I. Baskes, M.S. Daw, Embedded-atom-method functions for the fcc metals Cu, Ag, Au, Ni, Pd, Pt, and their alloys. Phys. Rev. B **33**, 7983 (1986)
28. A.F. Voter, S.P. Chen, Accurate interatomic potentials for Ni, Al, and Ni_3Al. Mater. Res. Soc. Symp. Proc. **82**, 175 (1999)
29. D. Bäuerle, *Laser Processing and Chemistry* (Springer, Berlin, 2000)
30. N.W. Ashcroft, N.D. Mermin, *Solid State Physics* (Holt, Rinehart and Winston, New York, 1976)
31. Z. Lin, E. Leveugle, E.M. Bringa, L.V. Zhigilei, Molecular dynamics simulation of laser melting of nanocrystalline Au. J. Phys. Chem. C **114**, 5686 (2010)
32. B. Rethfeld, K. Sokolowski-Tinten, D. von der Linde, S.I. Anisimov, Ultrafast thermal melting of laser-excited solids by homogeneous nucleation. Phys. Rev. B **65**, 092103 (2002)
33. D.S. Ivanov, L.V. Zhigilei, Effect of pressure relaxation on the mechanisms of short-pulse laser melting. Phys. Rev. Lett. **91**, 105701 (2003)
34. L.V. Zhigilei, B.J. Garrison, Microscopic mechanisms of laser ablation of organic solids in the thermal and stress confinement irradiation regimes. J. Appl. Phys. **88**, 1281 (2000)
35. G. Paltauf, P.E. Dyer, Photomechanical processes and effects in ablation. Chem. Rev. **103**, 487 (2003)
36. E. Leveugle, D.S. Ivanov, L.V. Zhigilei, Photomechanical spallation of molecular and metal targets: molecular dynamics study. Appl. Phys. A **79**, 1643 (2004)
37. N.A. Inogamov, V.V. Zhakhovskii, S.I. Ashitkov, YuV Petrov, M.B. Agranat, S.I. Anisimov, K. Nishihara, V.E. Fortov, Nanospallation induced by an ultrashort laser pulse. J. Exp. Theor. Phys. **107**, 1 (2008)
38. L.V. Zhigilei, Z. Lin, D.S. Ivanov, Atomistic modeling of short pulse laser ablation of metals: connections between melting, spallation, and phase explosion. J. Phys. Chem. C **113**, 11892 (2009)
39. E.T. Karim, Z. Lin, L.V. Zhigilei, Molecular dynamics study of femtosecond laser interactions with Cr targets. AIP Conf. Proc. **1464**, 280 (2012)
40. C. Wu, M.S. Cheristensen, J.-M. Savolainen, P. Balling, L.V. Zhigilei, Generation of sub-surface voids and a nanocrystalline surface layer in femtosecond laser irradiation of a single crystal Ag target. Phys. Rev. B **91**, 035413 (2015)